This is an original manuscript of an article published by Taylor & Francis in Quantitative InfraRed Thermography Journal (2019) on 16 May 2019, available online at:
https://www.tandfonline.com/doi/abs/10.1080/17686733.2019.1603824?journalCode=tqrt20
DOI*:* https://doi.org/10.1080/17686733.2019.1603824

Comparison of optimization strategies for the improvement of depth detection capability of Pulse Compression Thermography

H. Malekmohammadi[a]*, S. Laureti[a], P. Burrascano[a], M. Ricci[b]

[a] *Department of Engineering, University of Perugia, Polo Scientifico Didattico di Terni, Terni (TR), Italy*

[b] *Department of Informatics, Modeling, Electronics and System Engineering, University of Calabria, Rende (CS), Italy*

* hamed.malekmohammadi@unipg.it, Strada di Pentima 4, 05100, Terni, Italy

Comparison of optimization strategies for the improvement of depth detection capability of Pulse Compression Thermography

In Pulse Compression Thermography, the impulse response of the sample under test is retrieved pixelwise by applying a proper matched filter on the set of acquired thermal images obtained by stimulating the system with a heat source amplitude modulated by a proper coded signal. Linear frequency modulated chirp signals and binary codes are the most employed coded excitations, and to improve the detection capability of the technique, a non-linear frequency modulated chirp signal can be used to deliver more energy to sample in a wanted frequency range of interest. In this work, we report the application of an exponential chirp to modulate the heating source and we compare it with a standard linear chirp excitation. To do a fair comparison, various windowing functions have been applied on the matched filters to reduce range sidelobes, thus enhancing the retrieved impulse response quality. It is shown that the combined use of an exponential chirp and an appropriate matched filter obtained exploiting the Reactance Transform provides a faithful reconstruction of the sample impulse response and an enhanced signal-to-noise ratio with respect to the use of linear chirp. This has been demonstrated on a 3D-printed PMMA sample containing sixteen flat-bottom holes of different depths.

Keywords: pulse-compression, thermography, windowing, matched filter, 3D printed PMMA

1. Introduction

Active Thermography (AT) is a non-destructive evaluation technique employed in different research and industrial fields, such as material characterisation [1,2], defect detection [3], cultural heritage diagnostic [4-5] and food inspection [6]. AT always relies on exciting the sample under test with an external heating source to reach the desired thermal contrast.

So far, AT has been exploited in two main schemes: Pulsed Thermography (PT) and Lock-in Thermography (LT) [3,7,8]. In PT, a short time duration δ-like heating stimulus is used to excite the Sample Under Test (SUT) within an extended bandwidth. The features of interest are then extracted by analysing pixelwise both the heating and the cooling trend of the acquired impulse response $h(t)$. In LT the excitation is in a narrow frequency band but in wider time span, providing less information but increased Signal to Noise Ratio (SNR) with respect to PT.

In recent years, Pulse Compression Thermography (PuCT) [9-14] have been proposed and developed to both overcome the shortcomings and combine the advantages of LT and PT. In PuCT, a broadband coded heating stimulus is used to heat up the SUT. The main pros of using a coded signal to modulate the heating source emission is that its time duration and its bandwidth are uncorrelated: the signal duration can be increased while maintaining the bandwidth unaltered [15]. The SNR level can be thus enhanced quite arbitrarily by employing a sufficiently long coded signal.

In addition, both time and frequency-domain analyses can be performed effectively and contextually through PuCT: the Fourier analysis can be implemented on the acquired raw data while the time-domain analysis is performed on the output of the Pulse Compression (PuC) procedure, which consists on the application of a proper matched filter over the acquired raw thermogram time series to retrieve an estimate of the

impulse response $h(t)$ for each pixel. However, only an estimate $\tilde{h}(t)$ of the $h(t)$ is attained after PuC. This is because the employed coded excitation is both time- and band-limited so that an inherent mathematical noise is introduced by the procedure.

The mathematical noise introduced by PuC, and hence the quality of the retrieved $\tilde{h}(t)$ in the impulse response estimate, is usually quantified in terms of main-lobe width, i.e. range resolution, and sidelobes level, i.e. defect detection capability. These quantities strictly depend on (i) the effectiveness of the employed PuC algorithm, (ii) the time-frequency characteristics of the coded signal used and (iii) on the matched filter used for the compression. Concerning (i), recently Silipigni, et al. [14] proposed an optimized strategy to implement the PuC algorithm in PuCT. For point (ii), several references showed the pros and cons arising from the use of linear and nonlinear frequency modulated "chirp" signal and binary pseudo-noise sequences in PuCT [12,14,16-17]. However, there is still the need to investigate and compare the use of different matched filters (point (iii)) in terms of $\tilde{h}(t)$ quality in PuCT in combination with linear and non-linear chirp signals.

Despite the use of a baseband linear chirp signal represents the simplest and yet robust frequency modulated heating stimulus employed in PuCT, it has been shown that employing a tailored signal to deliver energy according to a target power spectrum, *e.g.* a non-linear chirp as in the present case, helps maximizing the energy spread at low frequencies, leading to an improved SNR for deeper defects [16-17]. Nevertheless, the $\tilde{h}(t)$ retrieved by using a baseband linear chirp is less prone to sidelobes with respect to the one obtained employing a bandpass non-linear chirp, thus resulting in a more accurate reconstruction of the ideal $h(t)$. Recently, P. Burrascano et al. [18-19], pioneered the use of the so-called Reactance Transformation to design an optimal matched filter in PuC applications relying on baseband chirp signals, which showed promises for a significant reduction of the sidelobes.

In this paper, a baseband linear chirp and a bandpass non-linear exponential chirp signals were exploited to modulate the emission of LED chips for inspecting a 3D-printed PMMA sample containing sixteen flat-bottom holes of different depths. The use of different matched filters was investigated, and their performances were qualitatively compared in terms of both $\tilde{h}(t)$ and thermograms and quantitatively in terms of SNR. It was shown that the combined use of a non-linear chirp signal with an optimal matched filter obtained from a Reactance Transformation maximised the detection capability of deeper defects while maintaining a high quality of the retrieved $\tilde{h}(t)$, hence higher SNR.

The paper is organised as follows: an introduction on Pulse Compression is given in Sec.2. Sec.2.1. provides details on linear and non-linear chirp signals. Sec.2.2. gives an insight on the different matched filters approaches used: Wiener Filter, Hann and Reactance-based windows. Sec. 3 explains the experimental setup and the SUT. In Sec. 4, the results will be shown and discussed and finally in Sec. 5 the paper will be concluded, and future prospects will be mentioned.

2. Theory of Pulse Compression

PuC is a measurement technique employed to estimate the impulse response $h(t)$ of Linear Time Invariant (LTI) systems in poor SNR conditions and it was firstly used in RADAR to improve the range resolution while maintaining the peak power of the sent signal relatively low [20]. In standard PT, flash lamps are usually exploited to heat the sample by means of a light pulse significantly shorter than the typical cooling time of the sample itself. Thus, the heating stimulus exciting the LTI system can be modelled as a Dirac's Delta function $\delta(t)$ so that for each pixel the corresponding impulse response

$h(j_x, j_y, t)$ is directly retrieved as the pixel temperature/emissivity time trend (see Fig.1(a)). Useful information about the sample are then obtained by analysing both the heating and the cooling trend of the $\{h(j_x, j_y, t)\}$ within a chosen range of interest T_h.

On the other hand, PuCT requires further processing steps to be performed, as it relies on the existence of two signals $\{s(t), \psi(t)\}$ such that their convolution $\tilde{\delta}(t)$ approximates the Dirac's Delta Function δ(t):

$$s(t) * \psi(t) = \tilde{\delta}(t) \approx \delta(t), \quad (1)$$

In the previous expression, "$*$" is the convolution operator, $s(t)$ is the input signal of duration T and bandwidth B, $\tilde{\delta}(t)$ is the PuC resolution function and $\psi(t)$ so called 'Matched' filter. The standard $\Psi(t)$ is noting but the time reversed replica of $s(t)$ however in the next Sections we will show that $\psi(t)$ must be modified to optimize the quality of the resolution function and hence of the PuCT.

Practically, in a PuC measurement protocol an estimate of the impulse response $h(t)$ of the LTI system is retrieved by using the coded signal $s(t)$ as input and by applying the $\Psi(t)$ on the output signal $y(t)$:

$$\tilde{h}(t) = y(t) * \psi(t) = \mathrm{h(t)} * \mathrm{s(t)} * \psi(t) \approx \mathrm{h(t)} \quad (2)$$

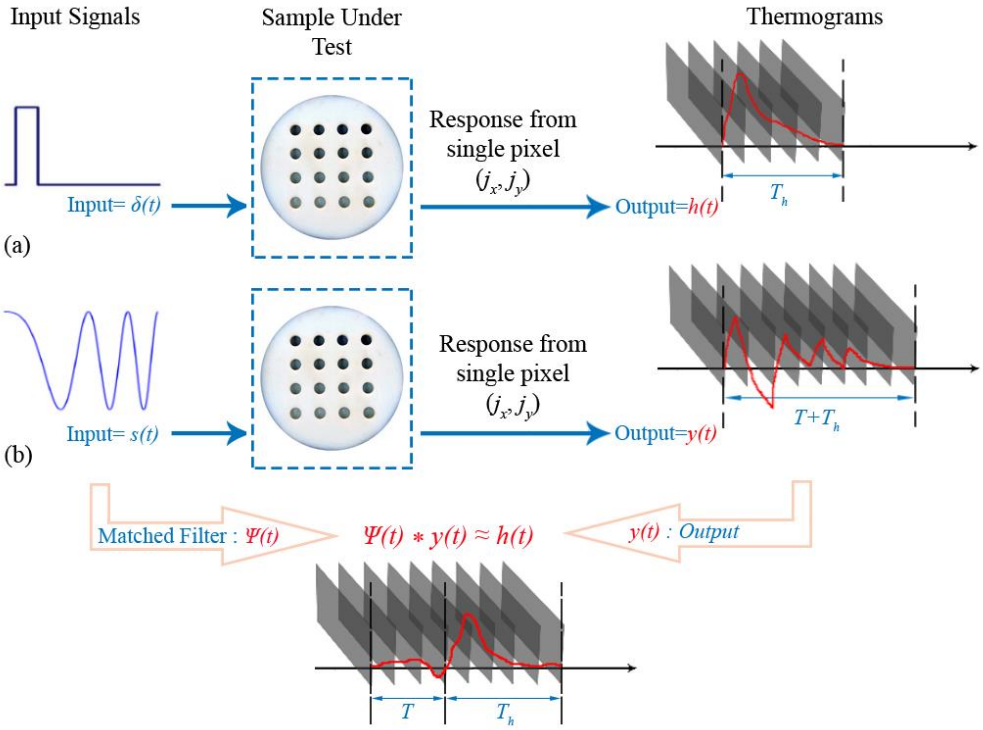

Figure 1. Comparison between (a) Pulsed Thermography (PT) and (b) Pulse-Compression Thermography (PuCT)

By assuming the lateral diffusion of the heat negligible, as commonly done in thermography, in PuCT an impulse response $\tilde{h}_{j,k}[\mathrm{n}]$ is estimated for each pixel of coordinate (x_j, y_k) where $\mathrm{s}_{j,k}[\mathrm{n}]$ is the pixel intensity/emissivity/temperature at the n-th frame, $\{\mathrm{n} \in [1, \mathrm{N}]\}$. Eq.(3) shows the process for a single pixel of the acquired image in the presence of an Additive-White-Gaussian-Noise (AWGN) as the $\mathrm{e}(t)$ term, uncorrelated to $\psi(t)$.

$$\begin{aligned} \tilde{h}(t) = y(t) * \psi(t) &= h(t) * \underbrace{s(t) * \psi(t)}_{=\tilde{\delta}(t)} + e(t) * \psi(t) \\ &= h(t) * \tilde{\delta}(t) + \tilde{e}(t) \approx h(t) + \tilde{e}(t) \end{aligned} \quad (3)$$

Fig.1 instead depicts a sketch of the PuCT procedure compared with that of PT: in PT the excitation is considered instantaneous and the sample's thermal impulse response is measured for a time T_h, which is the impulse response time duration, *i.e.* the time necessary for the diffusion of the heat. In PuCT, the sample is excited with a coded excitation of duration T and thermograms are collected for an overall time duration of $T + T_h$. After the application of the PuC algorithm, an estimated impulse thermal response of duration T_h is retrieved. Note that a step-heating contribute must be removed before applying successfully the PuC procedure [14].

2.1. Chirp Signals

A chirp signal is a frequency modulated signal whose instantaneous frequency varies linearly or non-linearly within a chosen range. A general mathematical definition of a chirp is given as:

$$s(t) = \sin\big(\phi(t)\big), \tag{4}$$

with $\phi(t)$ being the instantaneous signal phase [15,21]. The design of a chirp strictly depends on the definition of the instantaneous frequency $f_{ist}(t)$:

$$f_{ist}(t) = \frac{1}{2\pi}\frac{d\phi(t)}{dt} \tag{5}$$

For a linear chirp signal, the phase is a quadratic function $\phi(t) = f_0 t + \frac{B}{2T}t^2$, leading to $f_{ist}(t)$ that is a linear function of time:

$$f_{ist}(t) = f_0 + \frac{B}{T}t, \tag{6}$$

where B is the bandwidth $B = f_1 - f_0$, that is the difference between the initial and the final value of the instantaneous chirp frequency. Note that if $f_1 > f_0$, $B > 0$, therefore $f_{ist}(t)$ increases as time elapses and the chirp is called "up" chirp; otherwise if $f_1 < f_0$, then $f_{ist}(t)$ decrease as time elapses and the chirp is a "down" chirp. The chirp signals employed in this work are "up" ones.

When $\phi(t)$ varies neither linearly (i.e. a single-tone) nor quadratically, the resulting signal is a non-linear chirp. A non-linear chirp can be defined in two main ways: i) by starting from the trajectory of its $f_{ist}(t)$ in the desired range [f_0, f_1] and integrating it to retrieve the phase function $\phi(t)$; ii) or by starting from a target power spectrum following the procedure reported in [21]. In the present case, an exponential swept cosine non-linear chirp signal was used designed by following the procedure reported in Novak et al. [22]. Eq.(7) gives the analytical expression for the said signal:

$$s(t) = cos\left(2\pi f_0 L\left[e^{\frac{t}{L}} - 1\right]\right) \tag{7}$$

with L being the rate of the exponential increase in frequency that depends on T and the chosen f_1:

$$L = \frac{T}{log_e\left(\frac{f_1}{f_0}\right)} \tag{8}$$

For such signal, the expression of the $f_{ist}(t)$ and $\phi(t)$ are:

$$f_{ist}(t) = f_0 e^{\frac{t}{L}} \tag{9}$$

$$\phi(t) = 2\pi f_0 L\left[e^{\frac{t}{L}} - 1\right] \tag{10}$$

Note that Eq.(9) clearly shows that an exponential chirp cannot start from $f_0 = 0$, but must be bandpass. Except for this limitation, linear and non-linear chirp signals can be tailored to span a desired range of frequencies [f_0, f_1]. If on one hand the time duration

T of the coded excitation sets the overall energy sent toward the sample by the heating source considering a constant power, on the other hand the correct choice of f_0 and f_1 establishes and yet limits the maximum penetration depth within the SUT. Furthermore, f_0 and f_1 must be chosen to guarantee a sufficiently high $T \times B$ product. For these reasons, f_0 =0 Hz, f_1 =1 Hz and T = 80.0 s were chosen for the baseband linear chirp signal while the following values were selected for the exponential non-linear chirp: f_0 =0.01 Hz, f_1 =1 and T = 80.8 s. Please note that a special phase alignment condition was also considered for the employed exponential chirp, thus the effective time duration slightly differs with respect to the linear chirp one [22]. The two employed signals are depicted in Fig.2.

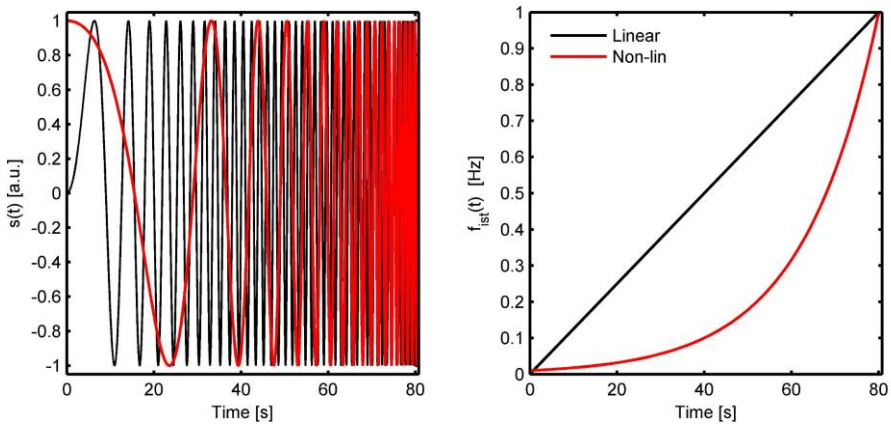

Figure 2. Plots of linear and non-linear chirp. Right: Linear (black) and non-linear (red) chirp signals, Left: $f_{ist}(t)$ versus time for the same signals

For a linear up-chirp, the instantaneous frequency slope is constant with time. On the other hand, the non-linear chirp instantaneous frequency is skewed toward the low frequency range, thus it can improve the defect detection capabilities for deeper defects since most of the delivered energy is on low frequencies. Nevertheless, baseband linear chirps exhibit in general lower sidelobe levels after PuC process than bandpass non-linear ones. Thus, a proper matched filter must be designed to reduce the sidelobe levels in non-linear chirp while improving the probing depth. The approaches used here to reduce the sidelobes are reported and described in the next section.

2.2. Problem of sidelobes and strategies to reduce them

The PuC's resolution depends on both $s(t)$ and $\psi(t)$. Since they are time-frequency limited signals, $\tilde{\delta}(t)$ is always an approximation of the ideal $\delta(t)$ and it is characterized by a main lobe of finite amplitude and width and by sidelobes of decreasing amplitude.

In general, the use of a matched filter $\psi(t)$ defined as time-reversal replica of $s(t)$ makes the spectrum of $\tilde{\delta}(t)$ to be real, since the phase of $\psi(t)$ maximizes the PuC output SNR at a specific time instant, which is the instant at which $s(t)$ is found possibly buried in noise on the acquired $y(t)$. The application of the matched filter over the recorded thermograms series performs a spectral phase correspondence. This in turn produces the desired PuC output peak at a given time instant and a spectral amplitude correspondence resulting in a maximized SNR at the said peak position. It can be shown that once the phase matching of $\psi(t)$ and $s(t)$ is assured, the filter response amplitude $|\Psi(f)|$ can be shaped to a specific aim, as for instance to maximize range resolution by using windows or to maximize the SNR of retrieved PuC output. For the latter, it can be demonstrated that employing $\psi(t) = s(-t)$ maximises the SNR obtained after PuC. On

the other hand, the so-obtained $\widetilde{\delta}(t)$ shows a high level of sidelobes, which hampers the faithful reconstruction of the thermal response of the SUT. Reduction in sidelobe levels can be realized by means of (i) different windowing functions $\alpha(t)$ on the matched filter, such that $\psi(t) = \alpha(t)s(-t)$ [15,23], or (ii) by exploiting a Wiener Filter approach to design an optimal $\psi_W(t)$ [14].

Regarding approach (i), the window function can significantly reduce sidelobes level at the cost of widening the main lobe. A lowpass Hann and a Reactance-based window have been applied here on the linear and non-linear chirp respectively. Please note that the Reactance-based window is applied only on the exponential non-linear chirp for its passband characteristic. The reader is referred to [19] for further details.

Concerning (ii), a possible method of decreasing the sensitivity of the PuC output to noise is to bound the frequency response of the matched filter $\Psi(f)$ according to a specific frequency selectively rule. To this aim, the Wiener filter approach is used here to design an optimal $\psi_W(t)$. $\psi_W(t)$ is described in frequency as in Eq.(11):

$$\psi_W(t) = IFFT\left(\frac{\Psi(f)}{|\Psi(f)|^2 + a + b \cdot |f|}\right), \tag{11}$$

where IFFT stands for Inverse Fast Fourier Transform operator, a and b are two regularization parameters, the former regulating the filter effect over the entire bandwidth, the latter penalizing the high frequencies. The employed value for the regularization parameters in this case was $a = b = 0{,}1$. Eq.(11) shows that the $\psi_W(t)$ has the same phase profile of the $\psi(t)$ but with modified spectrum amplitude so as to emphasize the frequency band in which the frequency spectrum of the $s(t)$ is known to be higher.

3. Experimental setup and sample under test

A National Instrument PCI-6711 Arbitrary Waveform Generator (AWG) board and a National Instrument 1433 Camera Link Frame Grabber were connected to a PC, and an ad hoc developed virtual instrument in LabVIEW managed the signal generation/acquisition. The AWG board provided both the wanted linear chirp excitation and a reference clock signal (CLK) for triggering the IR camera acquisition, which was a Xenics Onca-MWIR-InSb IR camera. A sketch of the experimental setup used is depicted in Fig.3:

The coded signal was input into a TDK Lambda GEN 750W power supply that fed eight LED chips placed at about 30 cm from the SUT. The LED chips are capable to provide a maximum overall power of 400W. The thermograms were acquired at 40 FPS.

SUT used in this experiment was a synthesized PMMA specimen manufactured by additive manufacturing method. The sample contains 16 flat-bottom holes of 10mm radius and various depths. A sketch of the sample is depicted in Fig. 4. The thermal

diffusivity of the sample was measured and is equal to 0.108 m^2/s. All measurements have been done on the defect-free surface as indicated in Fig. 4.

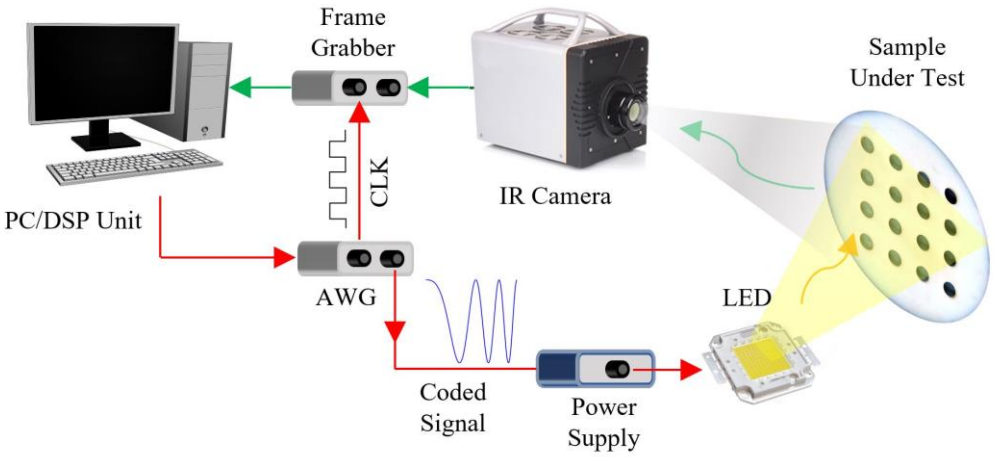

Figure 3. Sketch of the experimental setup

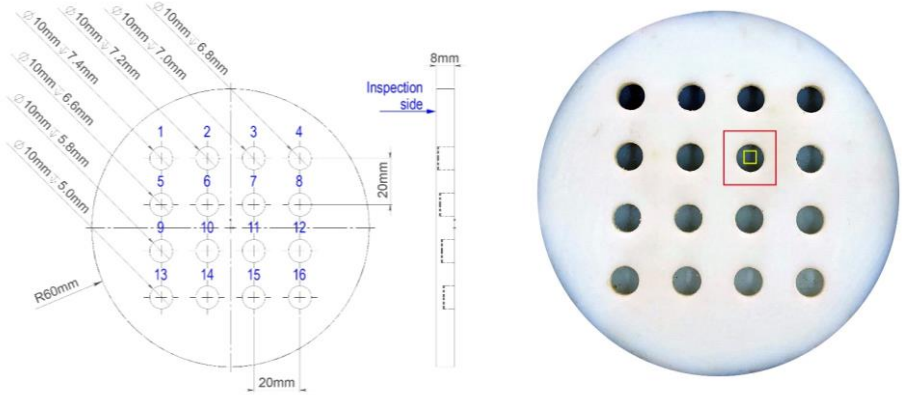

Figure 4. Sketch of the SUT (a) detailed drawing of the SUT containing 16 flat bottom holes with depths starting from 7.4mm depth with steps of 0.2mm. The defects have been numbered to be better distinguished. (b) The real image of the SUT after realization and the defected areas used for the SNR definition

4. Results and discussion

To compare the efficiency of the various strategies, the impulse response of the SUT in a certain point, i.e. seventh artificial defect, has been graphed. The impulse response was obtained using linear and non-linear chirp signals. For both linear and non-linear chirp, three cases were investigated: (i) without any windowing function and only using standard matched filter, (ii) by using Wiener filter instead of matched filter, (iii) with standard matched filter in combination with a window function. In case of linear chirp, a low-pass Hann window was used while in case of non-linear one the same Hann window was firstly modified by means of the reactance-transformation introduced in [18-19] and then applied to the matched filter. Fig. 5 depicts the graphs of the various impulse response trends obtained.

For the impulse response without any filter or window, the sidelobes are obviously visible. As expected, the use of the Wiener filter and the windowing functions reduced sidelobes but at the cost of wider main lobe.

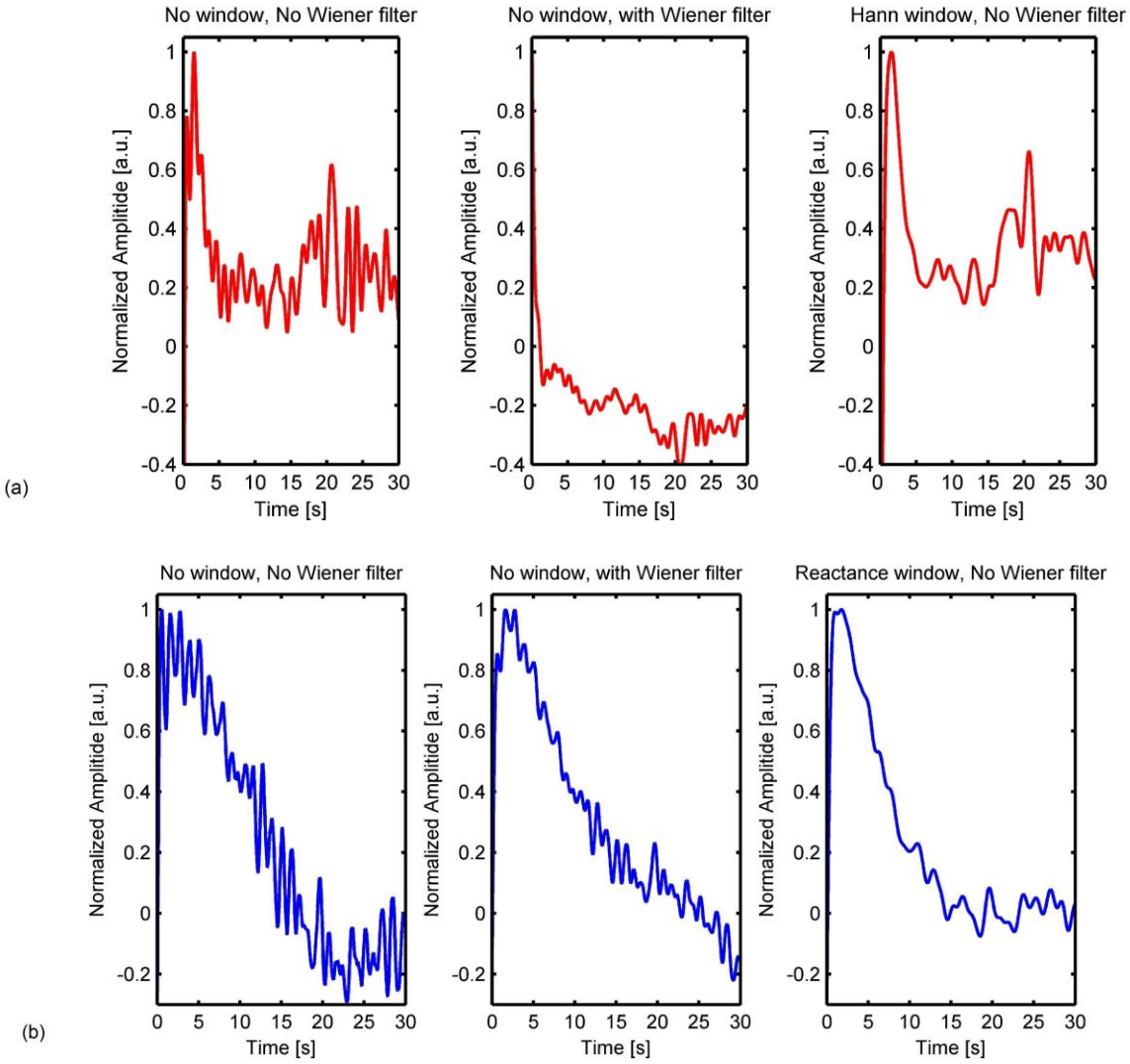

Figure 5. Comparison of the impulse responses obtained on the PMMA sample on defect number 7 by (a) linear chirp, (b) non-linear chirp. Results are depicted for the impulse response direct from PuC process (standards matched filter) without windowing and in combination with Wiener filter and windowing functions

For a quantitative comparison between the results and the validation of each strategy the SNR value in time has been used as the merit figure as follows:

$$SNR_k(t) = \frac{h_k(t) - \bar{h}(t)}{\sigma_h(t)} \tag{12}$$

where $h_k(t)$ is the impulse response of the k-th defect averaged over the region shown in Fig. 4(b) by the yellow box, $\bar{h}(t)$ is the impulse response averaged over the area shown in Fig. 4(b) by the red box and $\sigma_h(t)$ is its standard deviation over the same area.

Fig. 6 depicts the SNR values obtained for each proposed strategy. It can be seen that the SNR values are significantly improved by exploiting the exponential non-linear chirp with respect to linear chirp. The non-linear chirp in combination with reactance

window exhibits the best result. In case of the linear chirp, application of Wiener filter and the Hann window provides almost similar results in terms of SNR.

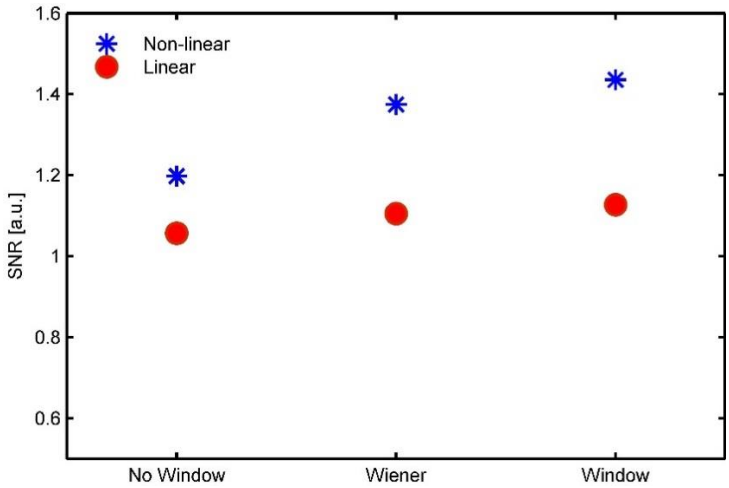

Figure 6. The graph of SNR values for different applied strategies on linear and non-linear chirp signals

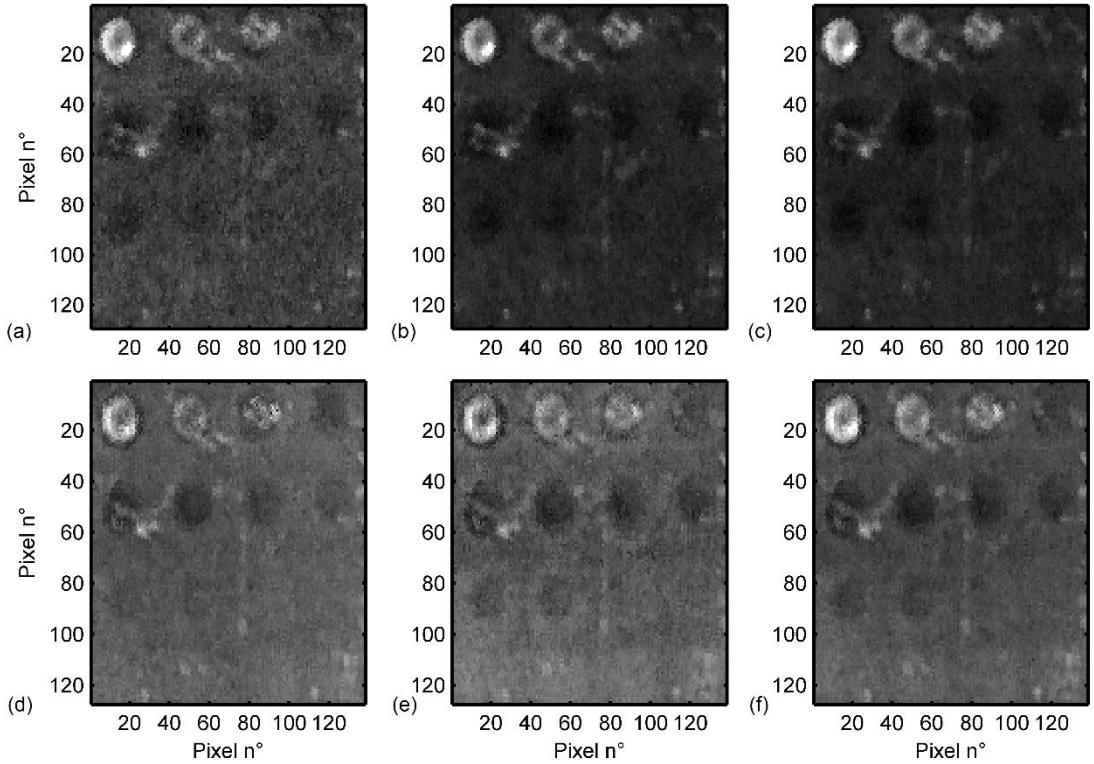

Figure 7. Thermograms acquired at the peak of SNR values for each strategy (a) to (c) respectively: exponential non-linear chirp without window and Wiener, with Wiener filter and without window, without Wiener and with reactance window, (d) to (f) respectively: linear chirp without window and Wiener, with Wiener filter and without window, without Wiener and with Hann window

After the calculation of the SNR values for each strategy, the thermograms corresponding to maximum value in time for each proposed strategy were found and depicted in Fig. 7, in which the thermograms in first row correspond to non-linear and second row to the linear chirp. One can obviously and qualitatively see the outcome of

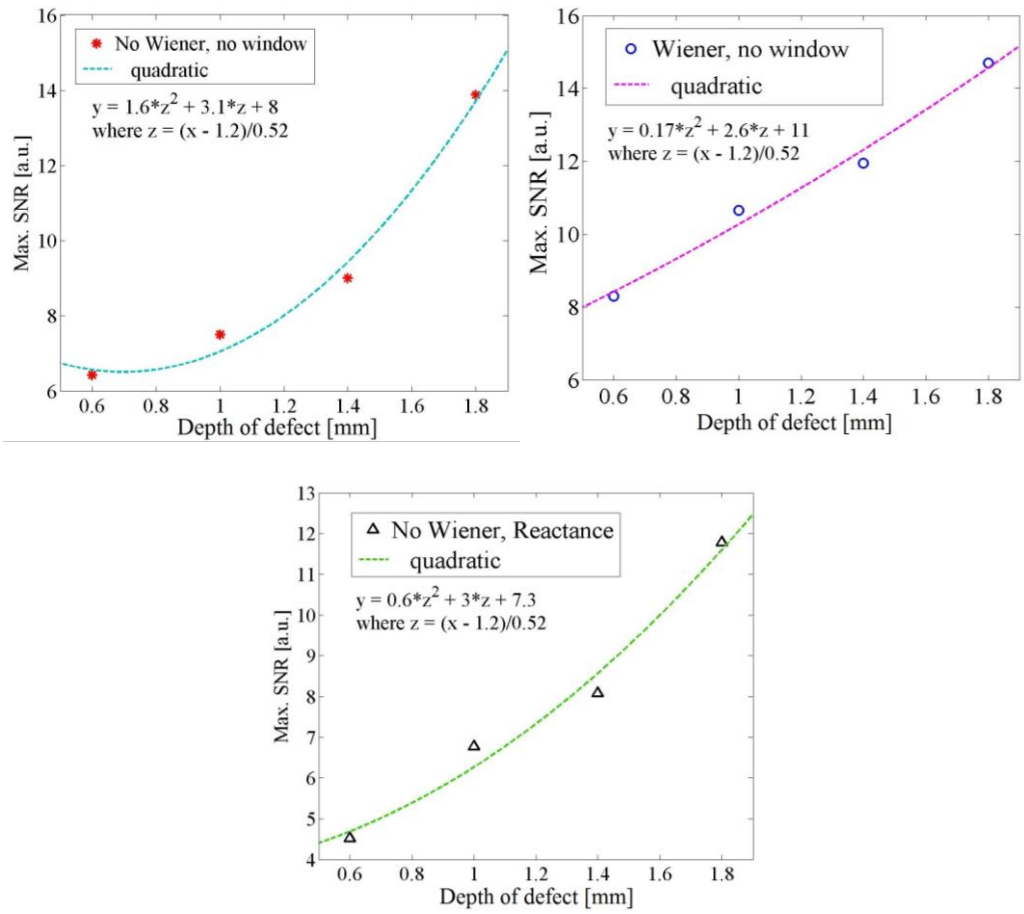

Figure 8. The relation between the SNR values and the defect's depth for different strategies along with the fitting data showing the quadratic relation between the SNR and the depth

the exponential non-linear chirp is more clear and deeper defects are visible with higher contrast which is in a good agreement with quantitative results.

Fig. 8 shows another quantitative evaluation of the results by plotting the SNR value for each strategy versus the defect's depth. The fitted curve shows a quadratic relation between these two values as expected.

5. Conclusion and future work

The use of a non-linear exponential frequency-modulated chirp signal in combination with a proper window improved the defect detection capability of deep defects in a pulse-compression thermography experiment implemented on a PMMA 3D-printed sample with artificial defects. The proposed approach can be easily extended to any frequency-modulated PuCT scheme were defects can occur in a quite wide range of depths requiring a broad range of excitation frequencies. Increasingly, the proposed procedure is still valid when sinusoidal chirps are replaced by squared frequency modulated signals. In conclusion, by combining long excitations typical of LT, and time-domain analysis proper of PT approach, the defect detection capability of the proposed PuC procedure can outperform that of more conventional techniques. Moreover, the reduction of the PuC sidelobes provides also a quite good quality for the reconstruction of the pixels' impulse responses so that PuCT can be also an effective alternative to PT even if the use of

advanced post-processing procedures specific of thermography must be used, such as TSR or partial least squares- based algorithms. As a future development, the exponential-chirp based PuCT procedure proposed here can be fully exploited by implementing also the analysis of eventual non-linear phenomena thanks to the peculiar characteristics of the exponential chirp definition [22].

Acknowledgement:
This research work has been partially supported from the European Union's Horizon 2020 research and innovation programme under the Marie Skłodowska-Curie grant agreement No 722134 – NDTonAIR.

References:

[1] Maldague X, Nondestructive evaluation of materials by infrared thermography. London: Springer; 1993.
[2] Meola C, Carlomagno GM, Giorleo L. The use of infrared thermography for materials characterization. J Mater Process Technol 2004; 155:1132–1137.
[3] Maldague X, Theory and practice of infrared thermography for nondestructive testing. Wiley series in microwave and optical engineering. Wiley 2001.
[4] Sfarra S, Ibarra-Castanedo C, Paoletti D, Maldague X. Infrared vision inspection of cultural heritage objects from the city of l'Aquila, Italy and its surroundings. Mater. Eval. 2013;71.5.
[5] Laureti S, Sfarra S, Malekmohammadi H, Burrascano P,et al. The use of pulse-compression thermography for detecting defects in paintings. NDT & E Int. 98 (2018); 147-154.
[6] Senni L, Ricci M, Palazzi A, Burrascano P, et al. On-line automatic detection of foreign bodies in biscuits by infrared thermography and image processing. Journal of Food Eng. 128 (2014); 146-156.
[7] Shepard SM. Advances in pulsed thermography. In: Proceedings of SPIE 4360, Thermosense XXIII, 511, 2001 March 23.
[8] Ibarra-Castanedo C, Bendada A, Maldague X. Image and signal processing techniques in pulsed thermography. GESTS Int Trans Com. Sci Eng. 2005; 22.1:89–100.
[9] Tuli S, Mulaveesala R. Defect detection by pulse compression in frequency modulated thermal wave imaging. Quantitative InfraRed Thermography Journal. 2005; 2.1:41-54.
[10] Mulaveesala R, Tuli S. Digitized frequency modulated thermal wave imaging for nondestructive testing.; Materials Evaluation 2005; 63.10.
[11] Tabatabaei N, Mandelis A. Thermal-wave radar: A novel subsurface imaging modality with extended depth-resolution dynamic range. Review of Scientific Inst. 2009; 80.3:034902.
[12] Mulaveesala R, Ghali VS. Coded excitation for infrared non-destructive testing of carbon fiber reinforced plastics. Review of Scientific Inst. 2011; 82.5:054902.
[13] Gong J, Liu J, Qin L, Wang Y. Investigation of carbon fiber reinforced polymer (CFRP) sheet with subsurface defects inspection using thermal-wave radar imaging (TWRI) based on the multi-transform technique. NDT & E Int. 2014; 62:130-136.
[14] Silipigni G, Burrascano P, Hutchins DA, et al. Optimization of the pulse

compression technique applied to the infrared thermography nondestructive evaluation. NDT&E Int; 2017, 87:100–110
[15] Hutchins D, Burrascano P, Davis L, Laureti S, Ricci M. Coded waveforms for optimised air-coupled ultrasonic nondestructive evaluation. Ultrasonics 2014; 54:1745–59.
[16] Dua G, Mulaveesala R, Siddique JA. Effect of spectral shaping on defect detection in frequency modulated thermal wave imaging. Journal of Optics 2015; 17.2:025604.
[17] Laureti S, Silipigni G, Senni L, et al. Comparative study between linear and non-linear frequency-modulated pulse-compression thermography. Applied Optics. 2018; 57.18: D32-D39.
[18] Burrascano, P, Laureti S, Ricci M, et al. Reactance transformation to improve range resolution in pulse-compression detection systems. 40th International Conference on In Telecom. and Signal Proc. (TSP). 2017; 480-483. IEEE, 2017.
[19] Burrascano, P, Laureti S, Senni L, Ricci M. Pulse Compression in Nondestructive Testing Applications: Reduction of Near Sidelobes Exploiting Reactance Transformation. IEEE Transactions on Circuits and Systems I: Regular Papers 99 (2018); 1-11.
[20] Klauder JR, Price AC, Darlington S, Albersheim WJ. The theory and design of chirp radars. Bell Labs Technical Journal 1960; 39.4:745-808.
[21] Pollakowski M, Helmut E. Chirp signal matching and signal power optimization in pulse-echo mode ultrasonic nondestructive testing. IEEE transactions on ultrasonics, ferroelectrics, and frequency control. 1994; 41.5: 655-659.
[22] Novak A, Simon L, Kadlec F, Lotton P. Nonlinear system identification using exponential swept-sine signal. IEEE Transactions on Instrumentation and Measurement, 2010; 59(8), pp.2220-2229.
[23] Pallav P, Gan TH, Hutchins DA. Elliptical-Tukey chirp signal for high-resolution air-coupled ultrasonic imaging. IEEE transactions on ultrasonics, ferroelectrics, and frequency control 2007; 54(8).